Orbit Determination for Mars Global Surveyor During Mapping

F. G. Lemoine,*
D.D. Rowlands and D. E. Smith
Laboratory for Terrestrial Physics
NASA Goddard Space Flight Center
Greenbelt, Maryland

D. S. Chinn,
D. E. Pavlis and S. B. Luthcke
Raytheon ITSS
Greenbelt, Maryland

G. A. Neumann and M. T. Zuber,
Department of Earth, Atmospheric, and Planetary Sciences
Massachussetts Institute of Technology
Cambridge, Massachusetts

Abstract

The Mars Global Surveyor (MGS) spacecraft reached its designated low-altitude, and near-circular orbit about Mars after termination of aerobraking on February 4, 1999. The Mars Orbiter Laser Altimeter (MOLA) returned its first data from this low-altitude orbit on March 1, 1999. The Doppler data acquired from the Deep Space Network were used to determine the orbit of the MGS spacecraft, so that the altimeter data could be used to map the topography of Mars. A detailed nonconservative force model was implemented for MGS that included articulation of the solar arrays. The tracking data in February and March 1999 were used to improve the knowledge of the Mars geopotential by developing MGM0964C20, a solution to 70x70 in spherical harmonics. When the improved nonconservative force model and the improved Mars gravity model, MGM0964C20, are applied in the MGS orbit determination during the mapping orbit, the overlaps of adjacent arcs in March 1999 show a consistency of 0.6 m in the radial direction, and 2 meters in total position. We demonstrate that altimeter crossovers from MOLA can be used to further improve the orbit determination for these arcs resulting in an orbit overlap consistency of 0.3 meters in the radial direction and 1.7 meters in total position.

INTRODUCTION

The Mars Global Surveyor (MGS) spacecraft reached a low-altitude near-circular orbit on February 4, 1999, after the termination of the second phase of aerobraking[1, 2]. The spacecraft carries the Mars Orbiter Laser Altimeter (MOLA) whose primary goal is to derive a global, geodetically referenced 0.2° x 0.2° topographic grid of Mars with a vertical accuracy of better than 30 meters[3]. During the interim science orbits in the Hiatus mission phase (October to November 1997) and the Science Phasing Orbits (March - April, and June - July 1998), 208 passes of altimeter data were collected by the MOLA instrument. Starting on March 1, 1999, MOLA obtained altimeter

*Code 926, Laboratory for Terrestrial Physics, NASA Goddard Space Flight Center, Greenbelt, MD 20771; E-mail: flemoine@olympus.gsfc.nasa.gov

measurements from the low-altitude mapping orbit. Altimeter data will be collected throughout the mapping phase of the MGS mission, or for at least one Mars year (687 days). Whereas the interim orbits of Hiatus and SPO were highly eccentric, and altimeter data were returned only when the spacecraft was below an altitude of 785 km, the MGS mapping orbit is near circular with altitudes ranging from 370 to 430 km. In the mapping orbit, altimeter data are returned continuously at a rate of 10 Hz.

Since the MGS orbit serves as a reference from which the topography of the planet is deduced, the proper analysis of the altimeter data requires that the orbits be known as accurately as possible. In this paper, we will discuss the force modelling required to achieve the best possible orbits during the mapping phase of the MGS mission.

DATA AND ORBIT DETERMINATION MODELLING

Mission Summary and Data Coverage

The MGS spacecraft was tracked by the antennae of the Deep Space Network (DSN) using two-way and three-way ramped Doppler, and two-way ramped range data[4, 5]. In addition, as described by Lemoine et al.[6], one-way Doppler data were obtained from the Ultrastable Oscillator (USO) aboard MGS during SPO-1 (March - April 1998) and SPO-2 (June - July 1998). No one-way Doppler data were used outside of these time periods. The MGS mission phases and orbit characteristics are summarized in Table 1.

After the end of aerobraking on February 4, 1999, most of February 1999 was devoted solely to acquisition of tracking data to allow for improvement of the gravity models of Mars. During this mission phase (known as the Gravity Calibration Orbit), the spacecraft was maintained in a quiescent state to minimize disturbances in the tracking and obtain as much high quality tracking data as possible.

A contingency period of science data collection took place in March 1999, prior to the deployment of the High Gain Antenna (HGA) on March 29, 1999. In this mode, (designated Fixed High-Gain Antenna Mapping) the spacecraft pointed its instruments at Mars 18 to 20 hours per day, and then turned toward the Earth four to six hours per day to return the science data, and obtain tracking. The first MOLA data after HGA deployment were obtained on April 2, 1999. After HGA deployment, normal mapping operations involved pointing the instruments at nadir while the High Gain Antenna independently tracked the Earth. The High Gain Antenna is located at the end of a two meter boom and two axis gimbals maintain the antenna pointed at the Earth over each orbit.

Mapping operations were interrupted on April 16, 1999 when the azimuth gimbal of the HGA became stuck at 41.5°. No MOLA altimeter data were collected from April 16 to April 28, 1999, while the causes of the anomaly were investigated. It was determined that the gimbal would not rotate further than 41.5°, precluding simultaneous collection of science data, and pointing of the High Gain Antenna at the Earth during certain phases of the mission.

Science data collection resumed on April 28, 1999. From April 28 to May 5, 1999, the spacecraft pointed the instruments at nadir to collect science data 18 to 20 hours per day, and then pointed the HGA antenna at Earth for four to six hours per day to transmit these data to the Earth. By May 5, 1999 the Earth-Mars-MGS relative geometry had changed sufficiently to allow resumption of normal mapping operations at least through February 2000.

Following, HGA deployment, a degradation in the quality of the tracking data was observed[7], including an increase in the data noise, as well as a 19 second periodicity in the tracking data. Thus, none of the tracking data after HGA deployment were used to help refine the models of the Mars geopotential.

Table 1: MGS Orbit Characteristics during MOLA Data Acquisition

Mission Phase	Dates	Orbital Period (hr)	Periapsis Ht. (km)	Periapsis Latitude (deg)
Insertion	September 12-16, 1997	44.993	263	31° N
Hiatus	Oct. 13 - Nov. 7, 1997	35.43	170	35° N
SPO-1	March 27 - May 1, 1998	11.64	171	61° - 71° N
SPO-2	May 28 - July 30, 1998	11.64	171	82° - 86.3° N 86.3° - 76° N
GCO & Mapping	February 4, 1999 - $\cdots$	1.97	377	90° S

Data Processing and Analysis

The GEODYN orbit determination program[8] was used to process the ramped Doppler and range observations for MGS. The modelling included use of the DE403 planetary ephemerides[9], in both the measurement and force models. In addition to the third body perturbations caused by the planets and the Sun, the third body perturbations due to Phobos and Deimos were also included, using a GM of 720,000 $\mathrm{m}^3/\mathrm{s}^2$ for Phobos[10], and 120,000 m^3/s^2 for Deimos[11] and the ephemerides of Jacobson[12]. The Mars radiation pressure was modelled using spherical harmonic models, as described by Lemoine[13], based on analysis of the Viking Infrared Thermal Mapper data. The formulation of Knocke et al.[14] was used to define the surface spots and the location of the source vectors for the Mars radiation pressure. The Mars radiation pressure is computed separately for 43 surface spots in three concentric rings and a central cap below the subspacecraft point that are in view of each spacecraft surface. The Stewart atmosphere model was used to compute the atmospheric density at the MGS altitude[15].

The Mars geopotential is modeled in spherical harmonics using the expression[16],

$$U = \frac{GM}{r} \sum_{l=0}^{\infty} \left(\frac{a_e}{r}\right)^l \sum_{m=0}^{l} \left\{ \bar{C}_{lm} \cos m\lambda + \bar{S}_{lm} \sin m\lambda \right\} \bar{P}_{lm}(\sin\phi) \tag{1}$$

where the expansion is defined using the spherical coordinates of radius, r, latitude, ϕ, and longitude, λ; $\bar{C}_{lm}$ and $\bar{S}_{lm}$ represent the normalized geopotential coefficients; $\bar{P}_{lm}$ are the normalized associated Legendre functions of degree l and order m; a_e is the reference equatorial radius; G is the universal constant of gravitation, and M is the planet mass. The 1991 IAU system of constants was used to define the orientation of Mars[17].

The *a priori* model was the MGM0890 solution, a model complete to 70x70, based on the historic Viking Orbiter and Mariner 9 S Band tracking, and the X Band tracking of MGS in the Hiatus and the Science Phasing Orbits [6]. Updated solutions to 70x70 were soon developed that incorporated the tracking from MGS in February and March 1999, and these improved models were applied in the production of orbits for analysis of the MOLA altimetry.

MGS periodically fires its thrusters to desaturate the reaction wheels, which absorb angular momentum from disturbance torques acting on the spacecraft. Three to four angular momentum desaturations occurred per day after entry into the low-altitude mapping orbit*. The thruster firings can impart some velocity impulse effectively altering the orbit. Since telemetry informs us of the time and duration of these events, the angular momentum desaturations are modelled using empirical three-axis accelerations. Constant radial, along-track, and cross-track accelerations are applied over the duration of each event (typically two to there minutes), and are estimated as part of each orbit determination solution.

*The AMD events are much more frequent in the low-altitude mapping orbit. In all of Hiatus, SPO-1, and SPO-2 only 29 AMD events were documented.

In the first pass through the February and March mapping orbit data, the tracking data were processed in one-day arcs. Later, as the modelling of the Mars geopotential improved, longer arcs (three to five days) were used. Each arc adjusted the spacecraft state, a solar radiation reflectivity coefficient (C_r), a drag coefficient (C_d) per day, as well as the empirical accelerations that modelled each AMD event.

Two distinct sets of orbit analyses were carried out. First, orbits that did not overlap were computed using the orbit modelling just described. These arcs in February and March formed the basis for the improvement in the modelling of the Mars geopotential. Second, quasi-reduced dynamic orbits that overlaped in time were computed to support the analysis of the MOLA altimeter data. These orbits adjusted additional empirical accelerations daily in the form of along-track once per revolution parameters. The adjustment of these extra empirical accelerations helps to remove residual orbit mismodelling. The orbit overlaps between adjacent arcs (except when orbit trim maneuvers occurred), provide a running check on the orbit quality. Since the frequent AMD events (three or four per day) would "interrupt" the period of each once per rev. empirical acceleration, constraint equations in GEODYN "tied" together the once-per-rev accelerations each day, effectively resulting in a single once-per-rev adjustment per day (See Rowlands et al.[18] for a description of the application of these constraint equations).

Nonconservative force modelling

The nonconservative force model must take into account the complex geometry and material properties of the spacecraft. The spacecraft is treated as a combination of flat plates arranged in the shape of a box, with attached solar arrays and drag flaps (ie. 'Box-Wing' or 'Macromodel'). The solar radiation pressure, atmospheric drag, and Mars radiation pressure forces acting on each plate are computed and vectorially summed to compute the total nonconservative force acceleration acting on the spacecraft. The Mars radiation pressure includes the reflected solar radiation, and the natural thermal emission of the planet. The same approach has been used to model the nonconservative forces acting on other spacecraft, for instance TOPEX/Poseidon[19], TDRSS[20], and GEOSAT-Follow-On[21]. Self-shadowing of spacecraft elements is not considered. A ten plate box-wing model for MGS was derived from engineering drawings of the spacecraft[22, 23]. The box-wing model included six plates for the spacecraft bus, and a total of four panels to represent the front and back sides of the +Y and -Y solar arrays. Each +Y or -Y panel is represented as a weighted sum of the area and material properties of the solar array yoke, the inboard solar array (which has gallium arsenide solar cells), the outboard solar array (which has silicon solar cells), and the drag flaps. The areas and reflectivities are summarized in Table 2. The reflectivity was assumed to be 80 percent diffuse and 20 percent specular. Multi-layer insulation (MLI) was assumed to cover the yoke and the spacecraft body. The spacecraft configuration in Feburary and March 1999 is depicted in Figure 1. In the spacecraft body-fixed frame, the +Z direction points at nadir, when MOLA is collecting data (MOLA, the Mars Orbiter Camera, and the Thermal Emission Spectrometer are located on the +Z face of the spacecraft bus). The +X direction is the axis through the stowed position of the High Gain Antenna.

The solar radiation pressure, Mars radiation pressure, and drag accelerations on Mars Global Surveyor are shown in Figure 2 for a 13 hour period starting at 11:00 on March 6, 1999. The dominant nonconservative force is the solar radiation pressure. The average total acceleration is 3.2 x 10^{-8} m/s^2 for the solar radiation pressure, 5.4 x 10^{-9} m/s^2 for the Mars radiation pressure, and 4.8 x 10^{-10} m/s^2 for the atmospheric drag. The Mars radiation pressure peaks in the vicinity of the subsolar point due to the concentration of the planet's thermal emission and reflected solar radiation on the sunlight hemisphere[13]. It is merely fortuitous that the atmospheric drag is relatively unimportant compared to the solar radiation pressure. The Mars areocentric longitude on March 6, 1999 was 107°, corresponding to summer in the northern hemisphere of Mars. Since Mars had past aphelion at this time, a substantial portion of the atmosphere had condensed onto the southern polar cap of

Table 2: MGS Macromodel Characteristics

Panel	Area (m^2)	Reflectivity	Comment
Solar Arrays			
Yoke	0.499	0.65	MLI.
Inner Panel (front)	3.077	0.11	GaAs cells.
Inner Panel (back)	3.077	0.43	44 % white paint; 56 % black substrate.
Outer Panel (front)	3.152	0.25	Si cells.
Outer Panel (back)	3.152	0.23	10 % white paint; 90 % black substrate.
Drag Flaps	1.418	0.15	black kapton.
Composite (front)	8.146	0.20	
Composite (back)	8.146	0.32	
Spacecraft Bus			
+X, -X	3.04	0.65	MLI.
+Y, -Y	3.37	0.65	MLI.
+Z, -Z	1.82	0.65	MLI.

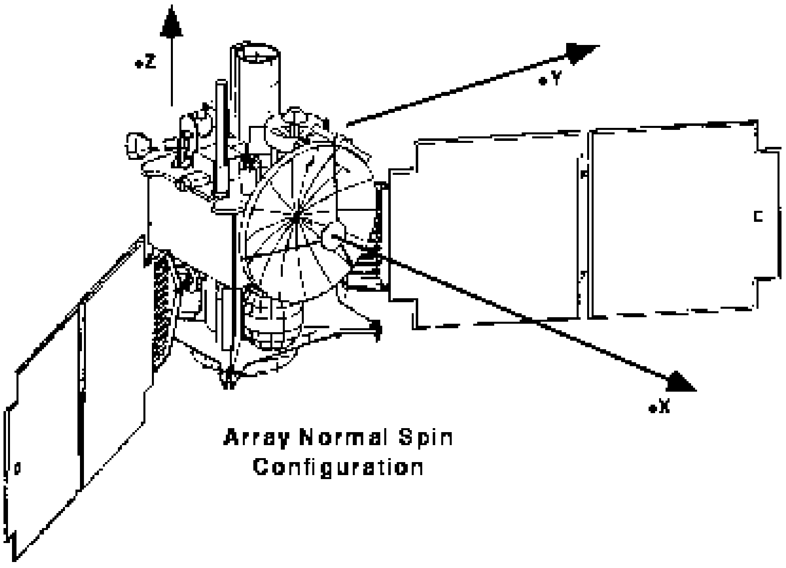

Figure 1: Nominal MGS spacecraft configuration during Array Normal Spin.

Mars, reducing the mean density at the MGS altitude (370 to 430 km). By early 2000, Mars will have past perihelion. This, in combination with the onset of summer in the southern hemisphere, means that the the southern polar cap will have largely sublimated, and the expected atmospheric density at the MGS altitude (and hence drag acceleration) will increase by a factor of 10 to 100[24].

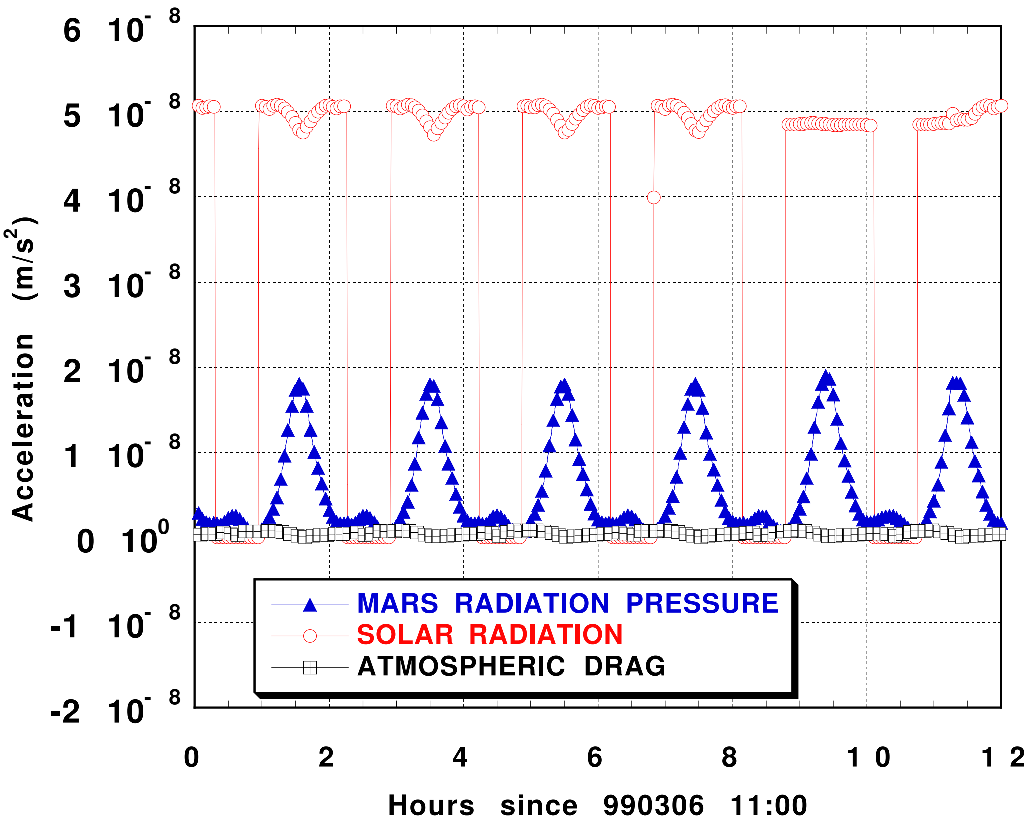

Figure 2: Nonconservative force model accelerations on Mars Global Surveyor computed from the MGS macromodel on March 11, 1999. The solar radiation pressure acceleration dominates at this time. The spacecraft operating mode affects the orientation of the solar arrays and the calculation of the solar radiation pressure. Through approximately 19:00 on March 11, the spacecraft was nadir pointing, and the solar arrays articulated, tracking the Sun. From about 19:00 through 22:00, the spacecraft was in Earth point and the solar arrays were held in a fixed orientation.

MGS Attitude Modelling

An essential component of properly modelling the nonconservative forces with a macromodel is to define the spacecraft attitude at all times. Since the solar arrays account for such a large surface area (16 m^2) on MGS, modelling their orientation as a function of time is also essential.

In February 1999, after entry into GCO, the spacecraft was maintained in Array Normal Spin (ANS). In this attitude, the spacecraft +X axis (containing the stowed High Gain Antenna) was pointed at the Earth, and the spacecraft rotated once every 100 minutes about this axis. The spacecraft solar arrays alternated between two fixed orientations, as depicted by the solar array quaternions in Figure 3 for the Y+ solar array.

During fixed HGA mapping in March 1999, the attitude regimes were more complicated. The spacecraft alternated between the collection of science data 18 to 20 hours per day (+Z axis pointed nadir), and collection of tracking data four to six hours per day (+X axis pointed at the Earth). During nadir pointing (mapping mode) the solar arrays articulated continuously, whereas during the Earth point regimes, the orientation of the solar arrays was held fixed. After deployment of the High Gain Antenna, the spacecraft remained nearly exclusively in nadir pointing (mapping) mode, with the exception of the period of the HGA anomaly (April 16 to April 28), and the second period of fixed High Gain Antenna mapping (April 28 to May 5, 1999).

Gaps in the telemetered spacecraft and solar array quaternions, caused some difficulties in the modelling of the spacecraft attitude. Our data processing with GEODYN required a complete time history of the quaternions over each orbital arc. The quaternions had to be preprocessed and prefiltered to fill in the gaps. Gaps of a few minutes could be easily filled with linear interpolation, providing sufficient accuracy for the macromodel and even the measurement model calculations. However, gaps of several revolutions had to be filled in by manufacturing the appropriate spacecraft or solar array quaternions using some knowledge of the spacecraft attitude control laws[†]. During fixed HGA mapping in March 1999, and again from April 28 to May 5 1999, the time of transition between the Earth point and nadir pointing regimes was not always obvious because of the gaps in the spacecraft quaternions. These transition times had to be inferred from other sources, such as the start and stop times of actual tracking, the start and stop times of altimeter data collection, and information in the mission sequence of events (SOE) files.

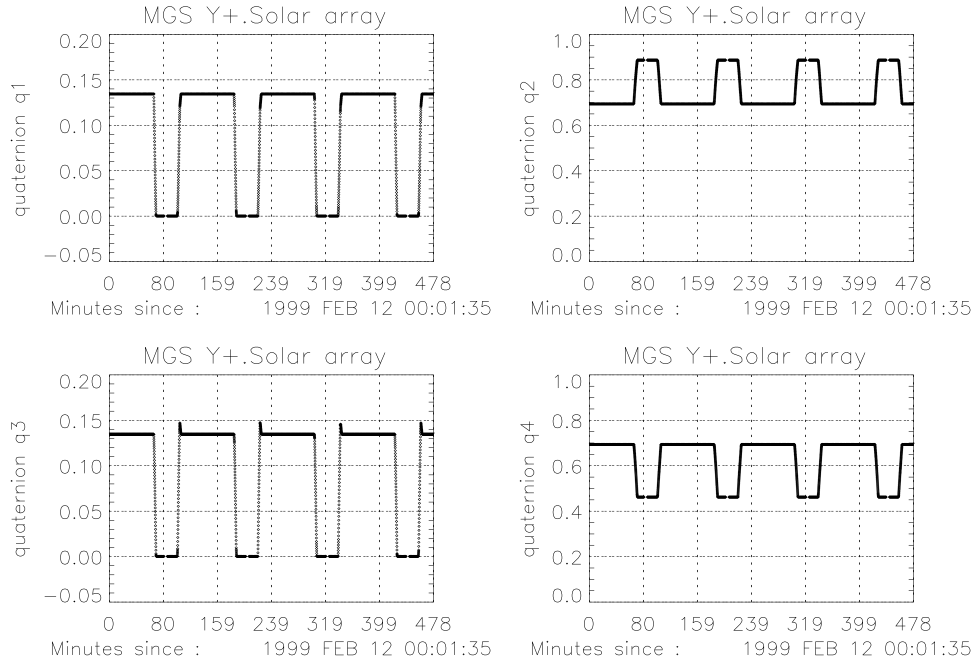

Figure 3: MGS Y+ solar array quaternions in GCO. The quaternions define the orientation of the Y+ solar array with respect to the spacecraft body-fixed frame. During GCO, the solar arrays alternated between two fixed orientations.

[†] While interpolation, or manufacture of quaternions during data gaps had sufficient accuracy for the macromodel and measurement calculations, geolocation of and analysis of altimeter data required the more precise pointing knowledge provided by actual data.

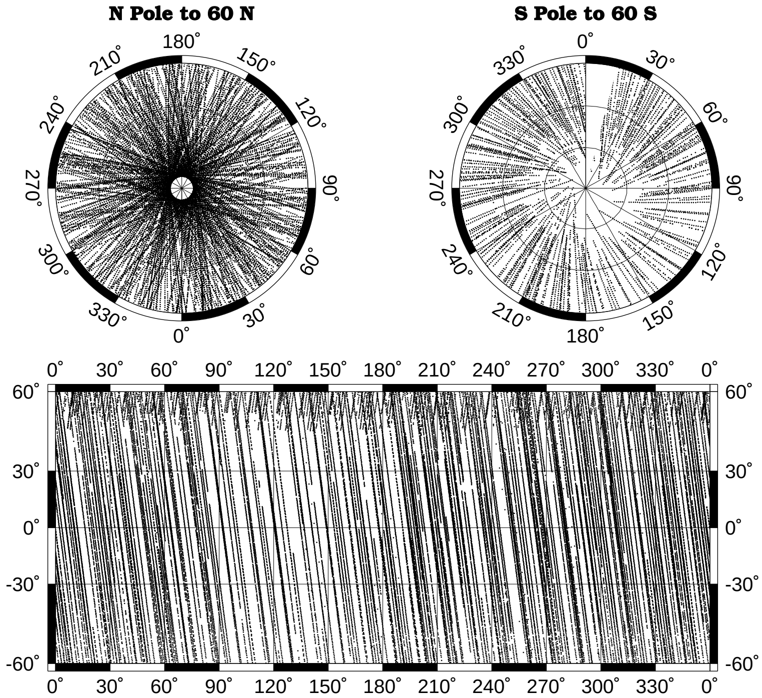

Figure 4: Doppler tracking coverage for Mars Global Surveyor from February 5, 1999 through March 27, 1999, after entry into the low-altitude mapping orbit, and prior to deployment of the High Gain Antenna.

GRAVITY FIELD IMPROVEMENT

Data Coverage

The coverage of the Doppler data from February 5, 1999 to March 27, 1999 is depicted in Figure 4. The coverage is mostly uniform over the entire planet. Some coverage is lacking over the southern polar regions because the spacecraft exited from occultation over this area. By the time lock up on the two-way Doppler signal occurred, the spacecraft had already moved further away from the South pole. Nonetheless, the coverage obtained by MGS in just two months is superior to the low altitude coverage obtained from the Viking Orbiters, which was limited to the equatorial regions of the planet (40° S to 40° N).

Method of Solution

Least squares normal equations were created for the tracking data in February 1999 and March 1999, and these normal equations were merged with the normal equations of the earlier MGS data from Hiatus and SPO, and the historical data from the Viking Orbiters and Mariner 9. The SOLVE program, a companion program to GEODYN which combines and manipulates normal equations, was used to obtain the least squares solutions [25]. No changes were made to the processing of

Table 3: Summary of Mars Gravity Solutions

Model	Include historical data	No. of observations Hiatus & SPO	Mapping	Effective Data Wt. (mm/s) Feb. 99	March 99	Kaula Power Law Applied
MGM0890	yes.	257,165	0	7.14	7.14	13.0 x $10^{-5}/l^2$
MGM0890I	yes.	257,165	66,605	7.14	7.14	13.0 x $10^{-5}/l^2$
MGM0964C5A	yes.	257,165	96,486	7.14	7.14	$\sqrt{2}$ 13.0 x $10^{-5}/l^2$
MGM0964C18	no.	257,165	96,483	0.36	7.14	$\sqrt{2}$ 13.0 x $10^{-5}/l^2$
MGM0964C20	no.	257,165	93,030	0.36	0.36	$\sqrt{2}$ 13.0 x $10^{-5}/l^2$

the historical Mariner 9 and Viking Orbiter data described in Lemoine et al.[6]. The Mars gravity solutions were computed using least squares collocation[26, 27]. An *a priori* Kaula-type power law constraint was applied in the derivation of the gravity solutions. The power law 13.0 x $10^{-5}/l^2$ was applied in the MGM0890 and MGM0890I solutions, whereas the power law $\sqrt{2}$ x 13.0 x $10^{-5}/l^2$ was used in MGM0964C5A, MGM0964C18, and MGM0964C20.

A sequence of solutions were developed that gradually included more data, and refined the models. This paper summarizes the performance of five landmark models developed at NASA GSFC that included the new tracking data from the MGS, low-altitude, mapping orbit:

1. MGM0890, the *a priori* model[6] to 70x70 that included MGS data from Hiatus and SPO, as well as the historical tracking.

2. MGM0890I, a solution to 70x70 that included 19 days of GCO data from February 4, 1999 through February 23, 1999, in the form of one-day arcs.

3. MGM0964C5A, a 70x70 solution that included all the available data in February and March 1999. The February data were processed in three day arcs, whereas the March data were processed in one-day arcs.

4. MGM0964C18, a refinement of the MGM0964C5A solution, where the MGS Doppler tracking data from February were upweighted from an effective weight of 7 mm/s to 0.357 mm/s.

5. MGM0964C20, a 70x70 solution derived from the normals were recreated based on data reductions using the MGM0964C18 solution and improved quaternion files for the spacecraft and the solar arrays. In this solution the February 1999 data were processed in three day arcs, whereas the March 1999 data were processed in four to five day arcs. Both the February and March 1999 data were weighted at 0.357 mm/s (0.01 Hz).

Whereas MGM0890, MGM0890I, and MGM0964C5A continued to incorporate the historical Mariner 9 and Viking Orbiter tracking. The MGM0964C18 and MGM0964C20 solutions only included the MGS data from Hiatus, SPO, and the low-altitude mapping orbit. The new MGS tracking data from the low-altitude, near-circular orbit completely supercede the historical data in both quality and coverage. Indeed, as will be shown it is possible to fit the historical data almost as well with MGS only gravity solutions (MGM0964C18, and MGM0964C20), as with solutions that incorporate the historical data (MGM0890I, MGM0964C5A).

Orbit performance measured by orbit overlaps

One gauge of the fidelity of the resultant geopotential models is to calculate the RMS difference in position between successive overlapping arcs. Three sets of overlaps were used:

Table 4: MGS Orbit Overlaps in February 1999

Model	Orbit Overlap Differences (m)[a]			
	Radial	Cross-track	Along-track	Total
MGM0890	41.72	10034.	432.98	10049.
MGM0890I	1.98	200.92	10.46	201.32
MGM0964C5A	0.80	220.86	7.65	221.10
MGM0964C18	0.35	77.88	3.40	78.04
MGM0964C20	0.18	42.64	2.02	42.72

[a]Average RMS of 12 overlaps.

Table 5: MGS Orbit Overlaps in March 1999

Model	Orbit Overlap Differences (m)[a]			
	Radial	Cross-track	Along-track	Total
MGM0890	38.53	196.56	156.53	266.23
MGM0890I	7.82	33.37	24.09	45.54
MGM0964C5A	2.28	20.30	6.74	22.68
MGM0964C18	1.34	19.84	5.51	21.06
MGM0964C20	0.60	5.28	2.01	6.26

[a]Average RMS of six overlaps.

1. Twelve overlaps of thirteen 30-hour arcs in February 1999. These arcs overlapped by six hours, and adjusted a drag coefficient (C_d) every eight hours, a solar radiation reflectivity coefficient (C_r), the spacecraft state, and the empirical accelerations for the AMD events (see Table 4).

2. Six overlaps of five to six day arcs in March 1999. These arcs adjusted a C_d per day, a C_r per arc, the spacecraft state, the empirical accelerations for the AMD events, and an empirical along-track acceleration per day (see Table 5). The overlaps average 2022 minutes in length, and on average 20 to 25 percent of each arc are in each pair of overlaps.

3. Eight overlaps of five to six day arcs in April through June 1999 (see Table 6). These arcs adjusted the same set of parameters as the arcs in the March 1999 overlap tests. These data are always independent (not included in the solution), whereas the data in February and March 1999 may or may not be independent, depending on the solution tested (see Table 3). These arcs are not as high quality as the arcs in February and March 1999 since (a) only a mean measurement offset was applied for the High Gain Antenna after deployment, and (b) the tracking data show evidence of greater noise following HGA deployment.

For consistency in these tests, all the results reported in Tables 4, 5 and 6 used the improved and refiltered solar array and spacecraft quaternions, even though the normals of the February

Table 6: MGS Orbit Overlaps after HGA deployment

Model	Orbit Overlap Differences (m)[a]			
	Radial	Cross-track	Along-track	Total
MGM0890I	11.89	113.48	234.80	263.01
MGM0964C5A	6.07	24.55	52.01	58.35
MGM0964C18	5.52	21.32	39.33	45.54
MGM0964C20	5.23	8.59	24.76	27.12

[a]Average RMS of eight overlaps in April, May and June 1999

and March 1999 data that contributed to the MGM0890I, MGM0964C5A, and the MGM0964C18 solutions used the first cut, unfiltered quaternions. The overlaps show that the weight selected for the tracking data plays an important role. Earlier solutions weighted the data too pessimistically at 7.14 mm/s (0.1 Hz). The X Band Doppler data have a precision of 0.1 mm/s, or better. Upweighting the data to 0.36 mm/s (0.01 Hz), as in the MGM0964C18 and in MGM0964C20 (see Table 3) allows these data to contribute more fully to the geopotential solution. The improvement observed with the MGM0964C20 field (in comparison to the antecedent solution, MGM0964C18) is due both to the reiteration, and also to the careful refiltering and reconstruction of the quaternions. Using the first set of quaternions (unfiltered) resulted in average overlaps using MGM0964C18 for the February data of 0.46 m in the radial direction, 108.84 m cross-track, 3.72 m along-track, and 109.05 m in total position. So simply switching quaternion sets improved the orbits (as reported in Table 4, the average radial overlap for the February data with the refiltered quaternions and MGM0964C18 is 0.35 m in the radial direction, and 78.04 m in total position). However, the second order improvement occurred with the development of the MGM0964C20 model. Nonconservative force mismodelling that had compromised the earlier solutions was removed in MGM0964C20.

The radial orbit overlaps with the latest MGM0964C20 solution in February and March 1999 are on average only a tens of cm. The dramatic radial consistency of the orbits is due not just to the fidelity of the gravity solution, but also the observing geometry. In February and March 1999 the tracking body (the Earth) was located from -4° to +14° above the MGS orbit plane. Thus, the MGS orbit was nearly edge-on as seen from the Earth. This edge-on geometry was propitious for maximizing the sensitivity to the Doppler data and to the determination of the MGS orbit in the radial direction. The overlaps are overall better in March (see Table 5) rather than in February 1999 (see Table 4). The adjustment of extra empirical accelerations in March 1999 compensates for the sparser tracking.

The overlaps are not shown following HGA deployment for the MGM0890 field (see Table 6). It is encouraging, that even with independent data (none of the post-HGA deployment data were used in the geopotential solutions), the total consistency of the orbits in all directions shows the same trends as the overlaps in February and March 1999.

Orbit performance measured by altimeter crossovers

Altimeter crossovers from MOLA were used to evaluate the geopotential solutions MGM0890I, MGM0964C5A, MGM0964C18, and the MGM0964C20. The altimeter crossovers have the advantage of being completely independent data, and are globally distributed. Altimeter crossovers were formed for four five to six day arcs from starting on March 7, March 13, March 18, and March 23, 1999. Between 940 to 980 crossovers were computed internally to each arc. No crossovers were formed if telemetered spacecraft quaternions were missing for either the descending or ascending track of a potential crossover point. The modelling of the altimeter crossovers is described in Rowlands et al.[28]. Altimeter crossovers from the highly eccentric orbits in SPO were used to estimate corrections to the preflight measurements of the orientation of the MOLA instrument with respect to the spacecraft frame[6, 28]. These new offset values of -0.0028° in roll,and -0.0086° in pitch were simply applied in the current tests with the mapping orbit altimetry. The crossovers are not used in these orbit determination solutions, which were determined solely from the range and the Doppler data for each gravity field model. The crossovers are editted for off nadir pointing angles, as well as the slope and the roughness of the terrain. Large crossover residuals (greater than 80 m) were eliminated. Because of the edit criterion of 80 m, the number of crossovers is not identical in all of the test arcs. The results are tabulated in Table 7 in aggregate for all four arcs. The crossovers show the same trend as the orbit overlaps, and the fits to the Doppler data. The crossover RMS is reduced as the fields are refined, and show the best performance with the MGM0964C20 field.

It is of interest to see whether the crossovers can still contribute to orbit improvement in the near-circular orbit. Crossovers were processed simultaneously with the Doppler tracking in four arcs

Table 7: MGS orbit performance measured by altimeter crossovers

Model	Doppler		Crossovers	
	No. of obs.	RMS (mm/s)	No. of obs.	RMS (m)
MGM0890I	14,838	18.93	3400	21.04
MGM0964C5A	14,838	1.65	3455	5.61
MGM0964C18	14,838	0.84	3449	5.57
MGM0965C20	14,838	0.53	3455	5.01

Table 8: MGS Orbit Overlaps with Altimeter Crossovers

Model	Orbit Overlap Differences (m)[a]			
	Radial	Cross-track	Along-track	Total
No Crossovers	0.59	0.81	1.83	2.17
With Crossovers	0.26	1.40	0.90	1.73

[a]Average RMS of three overlaps for four arcs from March 6, to March 23, 1999

of March 1999. Empirical once per revolution along-track accelerations were adjusted daily for these arcs, in addition to a drag coefficient per day, a reflectivity coefficient per arc, and the empirical accelerations for the AMD events. March 1999 is a particularly tough test for the crossovers since the Doppler data - although sparse, are of high quality. In addition, the Doppler data in March 1999 were used in the MGM0964C20 solution. The average RMS overlap is shown in Table 8 for the three overlaps of these arcs.

The addition of the crossover data improves the orbits overall, and especially in the radial, and the along-track directions. Some degradation is observed in the cross-track direction. It is especially encouraging that the consistency in the radial direction has been further improved from 0.59 to 0.26 meters. The use of these additional data in the form of altimeter crossovers allows extra empirical parameters to be adjusted - for instance cross-track once per revolution empirical accelerations - that would further improve these orbit consistency results.

RMS of fit to the Historical Data

Since we have used nearly all the available MGS data, the only quasi-independent data are the S Band data from the Viking Orbiters and Mariner 9. It is a necessary condition that the new models including MGS data obtain comparable fits to solutions based solely on the historical data, for instance the GMM-1[29], and Mars50c[30] solutions. Both GMM-1 and Mars50c are 50x50 solutions. A series of test arcs of the Mariner 9 and Viking Orbiter data were selected for each distinct orbital inclination and periapse altitude. The orbit geometry and the number of test arcs selected are listed in Table 9. All the orbits were highly eccentric, and the orbit periods ranged from 12 to 24 hours[13]. Two observations are readily apparent upon examination of the RMS of fit for these test arcs. First, the RMS of fit for all the new models with MGS is broadly similar to the GMM-1 and Mars50c models. In fact, for the low altitude periapse data (300 km), the fit to the Viking-1 and Viking-2 data is superior with the MGS derived models. Even the models that exclude all the historical data (MGM0964C18 and MGM0964C20) fit these low altitude data better than GMM-1 and Mars50c. The second observation pertains to the fit to the high altitude periapse data, in particular those from Mariner 9 and Viking Orbiter 1. Here the fits are degraded with the MGS derived models, compared to GMM-1 and Mars50c. So these results suggest an inconsistency in the long-wavelength gravity field to which MGS and the Viking Orbiters and Mariner 9 are sensitive. This inconsistency may reflect a discordance in reference frames, and an inadequacy in the 1991 IAU planet orientation model[17]. New solutions for the Mars orientation are available based on simultaneous analysis of Viking Lander and Pathfinder tracking which could be used instead of the

Table 9: Mariner 9 and Viking Orbiter Orbit Summary

Spacecraft	Periapse Ht. (km)	Inclination (deg)	No. of Test Arcs
Mariner 9	1600	64	6
Viking-1	1500	39	6
Viking-1	300	39	4
Viking-2	1500	55 & 75	2
Viking-2	800	80	7
Viking-2	300	80	9

Table 10: Mariner 9 and Viking Orbiter: RMS Summary

Orbit	Gravity Models: (RMS of fit in mm/s)						
	GMM-1	Mars50c	0890	0890I	0964C5A	0964C18	0964C20
Mariner 9	1.52	1.47	1.96	2.72	1.93	1.73	1.89
VO-1, 1500 km	2.36	2.42	2.35	2.56	4.20	4.20	4.03
VO-1, 300 km	1.77	1.55	1.48	1.63	1.74	1.54	1.62
VO-2, 1500 km	1.93	2.19	1.54	1.56	1.67	1.97	1.82
VO-2 800 km	1.84	1.80	1.79	1.85	2.82	2.41	2.00
VO-2 300 km	1.16	1.17	0.90	0.86	0.84	0.78	0.78

1991 IAU model.

Error Analysis

It is useful to project the predicted error from the gravity field covariances to 70x70, and ascertain the formal commission error due to uncertainties in the gravity field on the MGS orbit. These results are summarized in Table 11. The total radial error has decreased from 44 meters with MGM0890 to 8 to 10 cm with the MGM0964C18 and MGM0964C20 models. Similarly, the total error is reduced from 205 meters with MGM0890, to 1.6 to 2.0 meters with the latest MGS derived gravity models. These order of magnitude improvements in the predicted orbit error for MGS beg the question as to how realistic they really are. They certainly are a lower bound, since they omit the contribution of terms higher than degree 70. Unfortunately, other than the orbit overlap tests, we have no means to really test these orbit error predictions.

Some insight into the validity of the covariance may be gauged by examining the calibrations of the mapping orbit data in the geopotential solutions. As described by Lerch[31], the calibration factor measures the aggregate change in the geopotential coefficients divided by the aggregate change in the sigmas of these geopotential coefficients, when a set of data is removed from a geopotential solution. If the weighting of the data is appropriate, then the calibration factors should be close to unity. If the calibration factors are greater than unity, this is an indication that the set of data is contributing information inconsistent with the information supplied by the other sets of data in the solution. All things being equal, higher calibration factors suggest either overweighting of data or

Table 11: Mars Global Surveyor Predicted Orbit Error

Model	Orbit Error Projections (meters)			
	Radial	Cross-track	Along-track	Total
MGM0890	43.95	184.33	79.68	205.57
MGM0964C18	0.10	1.53	1.29	2.01
MGM0964C20	0.08	1.17	1.09	1.60

mismodelling problems with the data.

As discussed in Lemoine et al.[32], the calibration factors are averaged by degree or by order. The calibration factors were computed for the MGM0964C18 and the MGM0964C20 solutions, and are shown in Figure 5 and Figure 6. The average calibration factors for the mapping orbit data used in MGM0964c18 were: 1.082 (by degree), and 1.036 (by order). For the data used in the MGM0964C20 field, the calibration factors were 0.901 (by degree) and 0.818 (by order). Indeed, with MGM0964C20, the calibration factors suggest that the MGS data in February and March 1999 could even be slightly upweighted from 0.01 Hz (0.36 mm/s). The lower calibrations MGM0964C20 compared to MGM0964C18 are due to the improved nonconservative force modelling. Mismodelling of the nonconservative forces deleteriously affects the solution at the higher degrees and orders. Relatively high calibration factors at the lower degrees even with the MGM0964C20 model remain to be elucidated. By this internal consistency test, then the covariance of the MGM0964C20 solution is at least not overly optimistic.

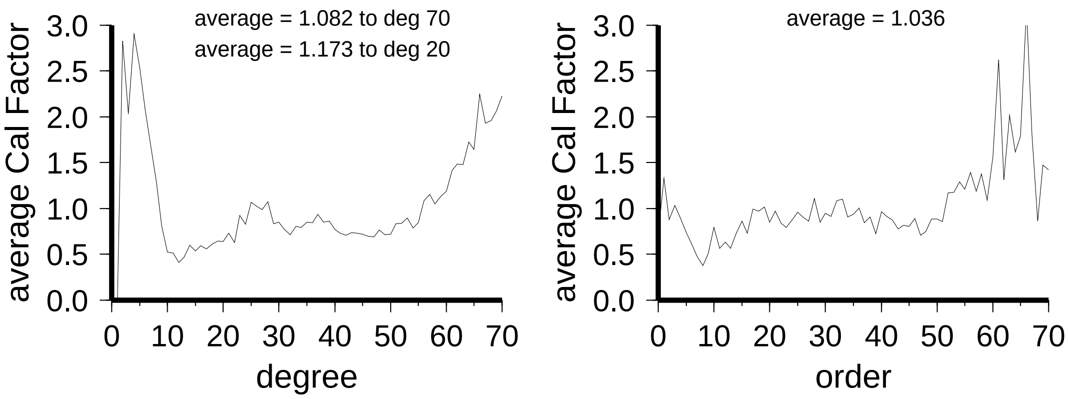

Figure 5: Calibration factors for the MGS mapping orbit data used in the MGM0964C18 solution.

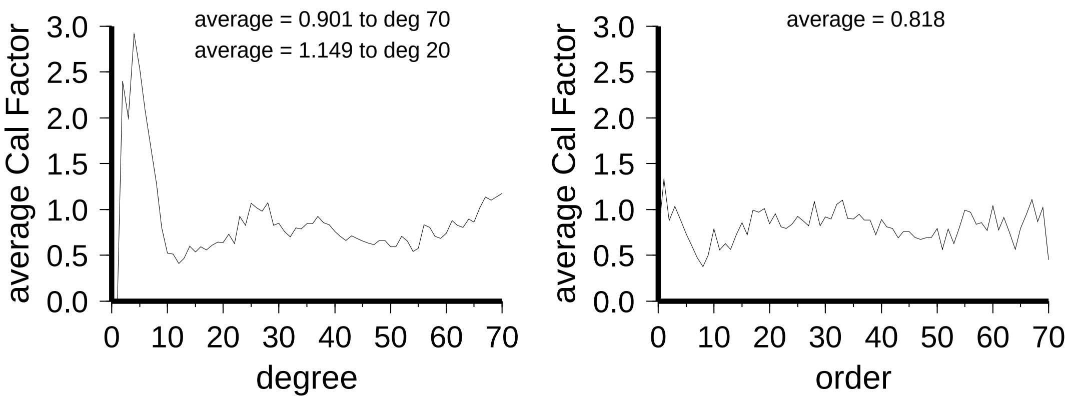

Figure 6: Calibration factors for the MGS mapping orbit data used in the MGM0964C20 solution.

SUMMARY

We have improved orbit modelling for Mars Global Surveyor in the low-altitude and near-circular mapping orbit by developing a detailed nonconservative force model for the spacecraft and by developing improved models of the Mars geopotential. A ten plate macromodel was developed for MGS. Telemetered spacecraft and solar array quaternions were used define the spacecraft attitude and solar array orientation in the macromodel. Two months of tracking data in February 1999 and March 1999 were processed using this macromodel. These data formed the basis for the order of magnitude improvement in the modelling of the Mars geopotential. The improved gravity model, MGM0964C20, a model complete to 70x70 in spherical harmonics results in arc to arc overlap consistency of a few meters in total position, and under a meter in the radial direction. One of the best gravity models available prior to entry in the mapping orbit, MGM0890, which included the MGS data from Hiatus and SPO, had arc to arc overlap consistencies of 38 to 40 meters in the radial direction and 220 to 260 meters in total position. Orbits were calculated used the improved nonconservative and geopotential modelling, and these orbits were distributed to the MOLA science team[‡].

The MOLA altimeter data were used validate the improvement in the Mars geopotential modelling. We have also demonstrated that the altimeter crossovers can be used in the near-circular mapping orbit to improve the orbit determination of MGS.

The single outstanding issue in orbit modelling for MGS remains properly correcting the Doppler data after deployment of the High Gain Antenna for the motion of the antenna over each orbit. Only a mean offset has been used so far in the data analysis for the MGS orbits following HGA deployment.

As stated in the MGS mission plan, tracking will consist of one 34-meter ground station pass per day, and one 70-meter ground station pass every third day[33]. Gaps of up to sixteen hours per day in the tracking will be possible, especially as the Deep Space Network faces increasing demands for its time from the Mars 1998 Orbiter and Lander, as well as other commitments. The incorporation of altimeter crossovers into the orbit determination for MGS will prove especially valuable, as the tracking becomes less dense. A second order benefit from the incorporation of crossovers, is that they will allow the adjustment of additional empirical parameters that will help to further remove residual errors in the orbit modelling.

ACKNOWLEDGEMENTS

We acknowledge Susan K. Fricke (Raytheon ITSS, Greenbelt) for data processing support, Jeffrey Schott (MIT and GSFC) for technical support, John J. McCarthy (Raytheon ITSS, Greenbelt) for aid with SOLVE. Trish Rodan (JPL), and Richard Simpson (Stanford University) provided useful mission and spacecraft information. We are grateful to Boris Semenov (JPL) and the Navigation Ancillary Information Facility for making available the MGS solar array quaternions.

References

[1] Albee, A. L., Mars Global Surveyor Mission: Status and Plan for Attaining the Circular Mapping Orbit, *EOS Trans. Am. Geophys. Un., 79*, 1998.

[2] Esposito, P. B., V. Alwar, S. Demcak, E. Graat, M. Johnston, and R. Mase, Mars Global Surveyor: Navigation and Aerobraking at Mars, *AAS Paper 98-384*, 1998.

‡These orbits refer the gdn-ql13.* series of orbits, and are available in NAIF-SPK format via anonymous ftp to geodesy.gsfc.nasa.gov (IP address 128.183.109.101); Change directory (cd) to dist/MGS/quick-look-orbits and fetch the gdn-ql13.* files.

[3] Zuber, M. T., et al., The Mars Observer Laser Altimeter Investigation, *J. Geophys. Res., 97*, 7781-7797, 1992.

[4] Moyer, T. D., Changes to the ODP and ODE for processing X-Band uplink data, *Jet Propulsion Lab. Eng. Mem., 314-430,* 1987.

[5] Moyer, T. D., REGRES Modifications for processing Block V exciter range observables, *Jet Propulsion Lab. Eng. Mem., 314, 5-1795,* 1995.

[6] Lemoine, F. G., et al. Precise Orbit Determination for Mars Global Surveyor During Hiatus and SPO, AAS Paper 99-147, *Spaceflight Mechanics 1999*, edited by R. H. Bishop, D. L. Mackinson, R. D. Culp, and M. J. Evans, 649-666, 1999.

[7] Sjogren, W. L., Jet Propulsion Laboratory, Personal communications, April 1999.

[8] Pavlis, D. E., S. Luo, P. Dahiroc, J. J. McCarthy, and S. B. Luthcke, GEODYN operations manuals, five volumes, Raytheon ITSS contractor report, March 26, 1999.

[9] Standish, E. M., X X Newhall, J. G. Williams, and W. M. Folkner, JPL Planetary and Lunar Ephemerides, DE403/LE403, JPL Interoffice Memorandum 314.10-127, Jet Propulsion Laboratory, Pasadena, California, May 22, 1995.

[10] Kolyuka, Y. et al. International project Phobos, experiment: Celestial mechanics, *Planet. Space Sci., 39*, 349-354, 1991.

[11] Williams, B. G., et al.,Improved determination of the Phobos and Deimos masses from Viking, Fall meeting of the American Geophysical Union, G21-A-11, San Francisco, December 1981.

[12] Jacobson, R. A., Mar033-5 Phobos and Deimos ephemerides description, Jet Propulsion Laboratory, Sept. 29, 1997.

[13] Lemoine, F. G., *The Dynamics of Orbiting Satellites and Gravity Model Development*, Ph.D. Thesis, The University of Colorado at Boulder, Boulder, Colorado, 1992.

[14] Knocke, P. C., Ries, J. C., and B. D. Tapley, Earth radiation pressure effects on satellites, *Proceedings of the AIAA/AAS Astrodynamics Conference*, Minneapolis, Minnesota, AIAA Paper 88-4292, 577-588, August 1988.

[15] Stewart, A. I. F., Revised time dependent model of the Martian atmosphere for use in lifetime and sustenance studies, Final report, JPL PO NQ-802429, Laboratory for Atmospheric and Space Physics, The University of Colorado, March 26, 1987.

[16] Kaula, W. M., *Theory of Satellite Geodesy*, Blaisdell, Waltham, Mass., 1966.

[17] Davies, M. E., et al., Report of the IAU/IAG/COSPAR working group on cartographic coordinates and rotational elements of the planets and satellites: 1991, *Celestial Mechanics and Dyn. Astr. 53*, 377-397, 1992.

[18] Rowlands, D. D. et al., Space Shuttle precision orbit determination in support of SLA-1 using TDRSS and GPS Tracking Data, *J. Astronautical Sciences, 45(1)*, 113-129, January-March 1999.

[19] Marshall, J. A. M., and S. B. Luthcke, Radiative Force Model Performance for TOPEXPoseidon Precision Orbit Determination, *J. Astronautical Sciences 42(2)*, 229-246, 1994.

[20] Luthcke, S. B., J. A. Marshall, S. C. Rowton, K. E. Rachlin, C. M. Cox, and R. G. Williamson, Enhanced radiative force modelling of the Tracking and Data Relay Satellites, *J. Astronautical Sciences 45(3)*, 349-370, 1997.

[21] Lemoine, F.G., D. D. Rowlands, N. P. Zelensky, S. B. Luthcke, C. M. Cox, and G. C. Marr, Precise orbit determination for the GEOSAT Follow-on spacecraft, *1999 Flight Mechanics Symposium, NASA/CP-1999-209235*, NASA Goddard Space Flight Center, 495-508, May 1999.

[22] Michael Griffin, Lockheed Martin Astronautics, Denver, Personal communications, January 1999.

[23] P. Tracadas, Massachusetts Institute of Technology, Personal communications, January 1999.

[24] Esposito, P. B., Mars Global Surveyor: Navigation Plan, JPL Document D-12002, Jet Propulsion Laboratory, Pasadena, California August 1996.

[25] SOLVE program guide to user input by R. E. Ullman, March 1993, Revised by John J. McCarthy for NASA GSFC, Code 926, Space Geodesy Branch; Raytheon ITSS Contractor report, Greenbelt, Maryland, August 1999.

[26] Schwartz, K. P., Least squares collocation for large systems, *Bull. Geod. Sci. 35*, 309-324, 1976.

[27] Schwartz, K. P., "On the application of least-squares collocation models to physical geodesy," in *Approximation Methods in Geodesy*, edited by H. Moritz and H. Sunkel, 89-116, H. Wichmann-Verlag, Karlsruhe, Germany, 1978.

[28] Rowlands, D. D., D. E. Pavlis, G. A. Neumann, and S. B. Luthcke, The use of laser altimeter in the orbit and attitude determination of Mars Global Surveyor, *Geophys. Res. Lett., 26(9)*, 1191-1194, May 1, 1999.

[29] Smith, D. E., F. J. Lerch, R. S. Nerem, M. T. Zuber, G. B. Patel, S. K. Fricke, and F. G. Lemoine, An improved gravity model for Mars: Goddard Mars Model 1, *J. Geophys. Res., 98(E11)*, 20871-20889, 1993.

[30] Konopliv, A. S., and W. L. Sjogren, The JPL mars gravity field, Mars50c, based upon Viking and Mariner 9 Doppler tracking data, *JPL Publication 95-5*, Jet Propulsion Laboratory, Pasadena, California, February 1995.

[31] Lerch, F. J., Optimum data weighting and error calibration for estimation of gravitational parameters, *Bull. Geod. 65*, 44-52, 1991.

[32] Lemoine, F. G., et al., *The Development of the Joint NASA GSFC and the NIMA Geopotential Model EGM96*, NASA/TP-1998-206861, NASA Goddard Space Flight Center, Greenbelt, Maryland, July 1998.

[33] Mars Global Surveyor Project: Mission Plan, Final Version, Rev. B (MGS 542-405), edited by Wayne Lee, Jet Propulsion Laboratory, Pasadena, California, November 1996.